Table 1 The dipole parameters best fitting the galaxy distribution

Flux (mJy)	N	Best δ ($\times 10^{-2}$)	Best ϕ (deg.)	Best θ (deg.)	$\chi^2_{\rm red}$
>40	125,603	1.4 ± 0.9	149 ± 49	135 ± 38	1.02
>35	143,524	1.7 ± 0.7	161 ± 44	117 ± 39	0.74
>30	166,694	2.2 ± 0.7	156 ± 32	88 ± 33	1.01
>25	197,998	2.2 ± 0.6	158 ± 30	94 ± 34	1.01
>20	242,710	2.1 ± 0.6	153 ± 27	93 ± 29	1.32
>15	311,037	1.5 ± 0.4	148 ± 29	59 ± 31	1.81
>10	431,990	1.0 ± 0.4	132 ± 29	25 ± 19	4.96

The table lists the best-fitting dipole model parameters (δ, θ, ϕ) together with 1σ errors for NVSS sources above various flux thresholds, after local sources have been removed. δ is expressed as a percentage. N is the number of sources left in the unmasked survey region and the reduced χ^2 values of the fit to the observed survey harmonics are also shown. The expected (CMB) velocity dipole parameters are $\delta = 0.9 \times 10^{-2}$, $\phi = 168°$, $\theta = 97°$. To find the best-fitting parameters, we vary the values of (δ, θ, ϕ) over a grid. For each set of parameters, we randomly generate a dipole galaxy distribution and mask it in the same way as the real data (below declination –40° and inside Galactic latitude 15°). We then measure the $A_{l,m}$ values of this test distribution, averaging over 100 realizations to increase accuracy. We hence obtain a mean and standard deviation for each $A_{l,m}$ in the set corresponding to the parameters (δ, θ, ϕ). We can then compute the χ^2 statistic with the observed survey harmonics. The best-fitting dipole parameters are found by minimizing χ^2; this minimum value (goodness-of-fit) indicates how well the dipole model fits the data. The errors on the best-fitting parameters are properly described by χ^2 contours in the parameter space. For example, with all three parameters varying, the 1σ and 2σ error regions are enclosed by χ^2 increases of 3.53 and 8.02.

(ref. 11). The local clustering dipole typically contributes $\Delta\delta = 0.5 \times 10^{-2}$ to the total amplitude.

The expected amplitude of the velocity dipole, assuming radio sources to have identical power-law spectra with flux density S depending on frequency ν as $S(\nu) \propto \nu^{-\alpha}$ and an integral source-count with N sources above S such that $N(>S) \propto S^{-x}$, is given by[2]:

$$\delta_{\rm pred} = 2(u/c)[2 + x(1 + \alpha)] \quad (3)$$

where u is the peculiar velocity of our reference frame with respect to the frame in which the radio source population is (assumed) isotropic, and c is the speed of light. CMB dipole measurements imply $u = 370 \pm 2\,{\rm km\,s^{-1}}$ (ref. 11). Taking $x \approx 1$ and a mean spectral index $\alpha \approx 0.75$, we find $\delta_{\rm pred} = 0.9 \times 10^{-2}$. Note that u is the peculiar velocity of the Sun in the CMB frame. (The speed of the Earth around the Sun is $\sim 30\,{\rm km\,s^{-1}}$ and can be neglected.) Our observed values of δ are on average 1.5σ away from this prediction.

We can be confident that our measured surface-density dipole is due to velocity rather than residual local clustering. Almost all the contribution to the local clustering dipole comes from redshifts $z < 0.03$—analysis of the IRAS PSCz dipole[6] shows that the dipole amplitude has almost converged by 100 Mpc. This result is verified in Fig. 3, where we plot the strength of the dipole contribution in redshift shells from the PSCz and RCBG3 catalogues. Furthermore, these catalogues contain almost all the radio galaxies to $z = 0.03$. This is demonstrated by Fig. 4, which gives magnitude–redshift plots for PSCz and RCBG3 galaxies matched with NVSS sources. The distributions make it clear that we are missing a negligible fraction of radio galaxies at $z < 0.03$.

It is hard to conceive of any other effect that could produce our measured dipole. A signal originating from instrumental or data-reduction effects would tend to skew the dipole direction towards the north or south poles, as such effects generally depend only on declination. However, our measured dipole points to declination approximately equal to 0°, in agreement with the CMB dipole. Moreover, instrumental effects should produce signal in higher (non-dipole) harmonics, but the best-fit dipole model is a good fit with $\chi^2_{\rm red} \approx 1$. Furthermore, the dipole amplitude is extremely unlikely to be a chance fluctuation of an isotropic universe. For example, for a flux-density threshold of 20 mJy, the isotropic universe ($\delta = 0$) model fits the observed harmonics with $\chi^2_{\rm red} \approx 2.28$, rejecting this model at a confidence level of >99.5%. It is difficult to see what else could produce the dipole, particularly one pointing (within the 1σ direction contours) in the CMB dipole direction. For the 20 mJy measurement, the 1σ confidence region for the direction encompasses just 5% of the sky.

The alignment of our measured velocity dipole with the CMB dipole supports the predictions of fundamental assumptions about the cosmological origin of the CMB, the linchpin of much present-day observational cosmology. This result indicates that objects at $z \approx 1$ (such as distant radio galaxies) can define the cosmic frame, and have an isotropic distribution in that frame. □

Received 11 October 2001; accepted 16 January 2002.

1. Smoot, G., Gorenstein, M. & Muller, R. Detection of anisotropy in the cosmic black-body radiation. *Phys. Rev. Lett.* **39,** 898–901 (1977).
2. Ellis, G. & Baldwin, J. On the expected anisotropy of radio source counts. *Mon. Not. R. Astron. Soc.* **206,** 377–381 (1984).
3. Scharf, C. *et al.* The 2–10 keV X-ray background dipole and its cosmological implications. *Astrophys. J.* **544,** 49–62 (2000).
4. Baleisis, A., Lahav, O., Loan, A. J. & Wall, J. V. Searching for large-scale structure in deep radio surveys. *Mon. Not. R. Astron. Soc.* **297,** 545–558 (1998).
5. Lahav, O. Optical dipole anisotropy. *Mon. Not. R. Astron. Soc.* **225,** 213–220 (1987).
6. Rowan-Robinson, M. *et al.* The IRAS PSCz dipole. *Mon. Not. R. Astron. Soc.* **314,** 375–397 (2000).
7. Condon, J. J. The NRAO VLA Sky Survey. *Astron. J.* **115,** 1693–1716 (1998).
8. Dunlop, J. S. & Peacock, J. A. The redshift cut-off in the luminosity function of radio galaxies and quasars. *Mon. Not. R. Astron. Soc.* **247,** 19–42 (1990).
9. Saunders, W. *et al.* The PSCz catalogue. *Mon. Not. R. Astron. Soc.* **317,** 55–64 (2000).
10. Corwin, H., Buta, R. & de Vacouleurs, G. Corrections and additions to the third reference catalogue of bright galaxies. *Astron. J.* **108,** 2128–2144 (1994).
11. Lineweaver, C. in *Proc. XVIth Moriond Astrophysics Meeting* 69–75 (Editions Frontieres, Gif-sur-Yvette, 1997).

Acknowledgements

We thank L. Miller and S. Rawlings for comments on early drafts. We also thank J. Condon for comments and suggestions.

Competing interests statement

The authors declare that they have no competing financial interests.

Correspondence and requests for materials should be addressed to C.B. (e-mail: cab@astro.ox.ac.uk).

Electrical discharge from a thundercloud top to the lower ionosphere

Victor P. Pasko*†, Mark A. Stanley†‡, John D. Mathews*, Umran S. Inan§ & Troy G. Wood§

* *CSSL Laboratory, Penn State University, University Park, Pennsylvania 16802, USA*
‡ *Langmuir Laboratory, New Mexico Tech, Socorro, New Mexico 87801, USA*
§ *STAR Laboratory, Stanford University, Stanford, California 94305, USA*
† *These authors contributed equally to this work*

For over a century, numerous undocumented reports have appeared about unusual large-scale luminous phenomena above thunderclouds[1–6] and, more than 80 years ago, it was suggested that an electrical discharge could bridge the gap between a thundercloud and the upper atmosphere[7,8]. Since then, two classes of vertically extensive optical flashes above thunderclouds have been identified—sprites[9–11] and blue jets[12–14]. Sprites initiate near the base of the ionosphere, develop very rapidly downwards at speeds which can exceed $10^7\,{\rm m\,s^{-1}}$ (ref. 15), and assume many

‡ Present address: Space and Atmospheric Sciences, Los Alamos National Laboratory, Los Alamos, New Mexico 87545, USA.

different geometrical forms[16–19]. In contrast, blue jets develop upwards from cloud tops at speeds of the order of 10^5 m s^{-1} and are characterized by a blue conical shape[12–14]. But no experimental data related to sprites or blue jets have been reported which conclusively indicate that they establish a direct path of electrical contact between a thundercloud and the lower ionosphere. Here we report a video recording of a blue jet propagating upwards from a thundercloud to an altitude of about 70 km, taken at the Arecibo Observatory, Puerto Rico. Above an altitude of 42 km—normally the upper limit for blue jets and the lower terminal altitude for sprites—the flash exhibited some features normally observed in sprites. As we observed this phenomenon above a relatively small thunderstorm cell, we speculate that it may be common and therefore represent an unaccounted for component of the global electric circuit.

The reported video recording was obtained during night-time observations using a Sony DCR TRV 730 charge-coupled device (CCD) video camera equipped with a blue extended ITT Night Vision GEN III NQ 6010 intensifier with a 40° circular field of view. The operation wavelength region of the intensifier was 390–870 nm at 77% sensitivity and 350–890 nm at 44% sensitivity. The intensifier provided a monochrome (predominantly green) image output. The camera was deployed at the Lidar Laboratory of Arecibo Observatory, Puerto Rico (18.347° N, 66.754° W, elevation 305 m above the sea level) (Fig. 1).

In the late evening of 14 September 2001, a cluster of thunderstorm cells developed at approximately 200 km range northwest of the observation site. Figure 1 shows an infrared image acquired from the GOES 8 satellite at 03:15 UT on 15 September 2001. The storm cloud top and the associated, almost continuous, lightning activity were clearly seen by the naked eye from Arecibo Observatory. The lower edge of the camera's field of view was aligned with the distant cloud top (altitude approximately 16 km) to avoid penetration of the direct light from bright lightning channels into the intensifier. The exact pointing direction of the video camera for the event was determined using the recorded star field (azimuth 336°, elevation 19.8°, corresponding to the centre of the camera field of view). GPS time stamps were recorded using the same video camera several hours before and several hours after the reported event, providing timing information with ±33 ms accuracy.

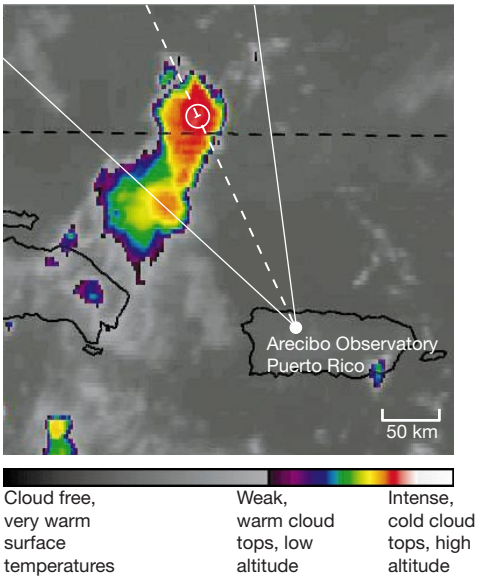

Figure 1 GOES-8 infrared image. This infrared image (1 km resolution) of the Puerto Rico region was acquired from the GOES-8 satellite at 03:15 UT on 15 September 2001 (http://wwwghcc.msfc.nasa.gov).

The event was observed starting at 03:25:0.782 UT on 15 September 2001, lasted a total of 24 video frames (~33 ms each), and concluded with an intense lightning flash in the underlying thundercloud in frame 25. Figure 2 shows a sequence of nine images extracted from frames 6–14. The full video sequence, including odd and even video fields for each frame, is available as Supplementary Information.

Figure 1 shows the camera's pointing direction and field of view. The dashed line represents the direction toward the apparent starting point of the event in frame 1 (see Supplementary Information), which intersects the coldest (and hence highest) cloud tops at ~200 km range. The 20-km-diameter circle drawn around the intersection point corresponds to the estimated transverse dimension (at ionospheric altitudes) of the observed phenomena. The maximum uncertainty in the estimated range of ~200 km is ±20 km, corresponding to the width of the thunderstorm region, which translates to a ±2 km altitude uncertainty of features shown in Fig. 2, too small to affect any conclusions reported here.

The apparent speed of upward propagation of the observed phenomena remained remarkably stable during the first five frames, and is estimated to be 0.5×10^5 m s^{-1} ($\pm0.07\times10^5$ m s^{-1}), consistent with known speeds of the leader process in conventional lightning[20]. The speed increased to 1.6×10^5 m s^{-1} between frames 5 and 6, and to 2.7×10^5 m s^{-1} between frames 6 and 7. The analysis of the two video fields corresponding to frame 8 indicates that the large altitude change between frames 7 and 8 happened in two steps. During the first field the left branch, clearly visible in frame 7, extended up to altitude ~70 km, while during the second field the right branch formed with a wider tree-like structure. The altitude change of ~32 km for the left branch and ~37 km for the right branch happened faster than the duration of one video field (16.7 ms). The estimated speed in the range $(1.9–2.2)\times10^6$ m s^{-1} is therefore a lower bound on the actual speed, which was probably higher.

The electromagnetic signatures of lightning discharges ('sferics') associated with the observed luminous event were recorded at two

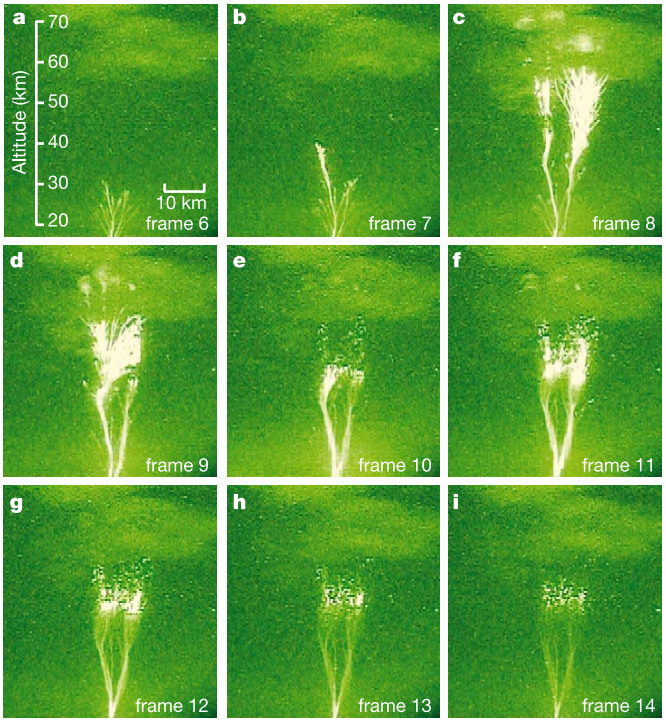

Figure 2 The time dynamics of the reported luminous event. Panels **a**–**i** correspond, respectively, to frames 6–14 as discussed in the text.

locations: Dominguito (18.421° N, 66.740° W), Puerto Rico, and at Palmer Station (64.774° S, 64.054° W), Antarctica. Dramatic rebrightening of the event was observed in frames 18 and 25 (see Supplementary Information) in association with large sferics. The sferic polarity indicated an upward transport of negative charge during the rebrightening. Also, an upward motion of subsequent breakdown was clearly evident between frames 18 and 19 (see Supplementary Information). As it is commonly known that subsequent breakdown of a given polarity in lightning generally occurs in the same direction as the initial breakdown of the same polarity, it is likely that the jet itself was created by upward negative breakdown, as was first suggested in ref. 28. A detailed report on the electromagnetic signatures will be presented elsewhere.

The apparent diameter of the breakdown filaments in the recorded images is estimated to be 1.26 km (±0.26 km), similar to the estimated diameters of stars recorded in the same images. Thus our video recordings cannot be used to reliably estimate the minimum scale of the structure, although they provide conclusive evidence for the presence of filamentary branching structure as an essential component of the observed phenomena. This finding agrees with a recently reported colour photograph showing details of streamers in blue jets[14], and provides the most detailed evidence presented to date of the theoretically predicted internal streamer structure of blue jets[21–23].

The transition apparent in frame 10 between the upper region dominated by hotspots and the lower region dominated by relatively smooth filamentary structure is estimated to be at an altitude of 42 km. This transition height is similar to the normal upper terminal altitude of blue jets and the lower terminal altitude of sprites.

The upward branches of the reported phenomena exhibit a diffuse termination at an altitude of approximately 70 km in frame 8. The 70 km termination closely coincides with the steep ledge of the lower ionospheric conductivity profile typically recorded during night-time rocket measurements in equatorial regions (for example, in Kenya[24] and Peru[25]).

The initial stage of the observed phenomena closely resembles the general geometrical shapes and propagation speeds of previously documented blue jets[12–14], and the event was seen visually to be blue in colour. We therefore speculate that it can be classified as a blue jet, which propagated upward beyond the previously documented altitude. Our results represent, to our knowledge, the first video observation of blue-jet phenomena from the ground, although we emphasize that the possibility of such observations was demonstrated by previous ground-based video recordings of blue starters[26], which are probably related to the initial phases of blue jets[23,27].

The subsequent dynamics of the upper part of the phenomenon closely resembles some of the features often observed in sprites[15–17] (that is, the shape of branching discharge trees, the diffuse termination of the breakdown branches on the lower ionospheric boundary, the evolution of the discharge trees into hotspots, and the high propagation speed). We note also that there are some similarities in visual appearance of the observed phenomenon and the so-called palm-tree events, which follow the occurrence of large groups of sprites and exhibit the same red colour as sprites[18,19]. However, some other features of the observed phenomenon, such as its long duration, the altitude extent, and no apparent association with a positive cloud to ground lightning discharge, do not match typical properties of sprites.

The phenomenon we report here, which effectively demonstrates that an electrical contact between the thundercloud and the lower ionosphere was established in this event, may have been facilitated by the relatively low night-time middle atmospheric conductivity typically observed in the tropics[24,25]. The lower conductivity values correspond to longer dielectric relaxation timescales (that is, ϵ_o/σ, where ϵ_o is the permittivity of free space and σ is the conductivity), and therefore allow easier penetration of quasi-static thundercloud electric fields—which presumably drive the observed phenomena[23]—to higher altitudes. Given the fact that the phenomenon was produced by a relatively small (~2,500 km^2) thunderstorm cell, such cloud-to-ionosphere discharges may be very common in the tropics and may constitute an important, but as yet unaccounted for, component of the global electric circuit[29,30]. □

Received 6 November 2001; accepted 24 January 2002.

1. Wood, C. A. Unusual lightning. *Weather* **6,** 64 (1951).
2. Wright, J. B. A thunderstorm in the tropics. *Weather* **6,** 230 (1951).
3. Vaughan, O. H. Jr & Vonnegut, B. Lightning to the ionosphere? *Weatherwise* 70–72 (April, 1982).
4. Vaughan, O. H. Jr & Vonnegut, B. Recent observations of lightning discharges from the top of a thunderstorm into the clear air above. *J. Geophys. Res.* **94,** 13179–13182 (1989).
5. Hammerstrom, J. G. Mystery lightning. *Aviat. Week Space Technol.* (30 August, 1993).
6. Rodger, C. J. Red sprites, upward lightning, and VLF perturbations. *Rev. Geophys.* **37,** 317–336 (1999).
7. Wilson, C. T. R. The electric field of a thundercloud and some of its effects. *Proc. Phys. Soc. Lond.* **37,** 32D–37D (1925).
8. Wilson, C. T. R. A theory of thundercloud electricity. *Proc. R. Soc. Lond. A* **236,** 297–317 (1956).
9. Franz, R. C., Nemzek, R. J. & Winckler, J. R. Television image of a large upward electrical discharge above a thunderstorm system. *Science* **249,** 48–51 (1990).
10. Sentman, D. D., Wescott, E. M., Osborne, D. L., Hampton, D. L. & Heavner, M. J. Preliminary results from the Sprites94 campaign: Red Sprites. *Geophys. Res. Lett.* **22,** 1205–1209 (1995).
11. Lyons, W. A. Sprite observations above the U.S. high plains in relation to their parent thunderstorm systems. *J. Geophys. Res.* **101,** 29641–29652 (1996).
12. Wescott, E. M., Sentman, D. D., Osborne, D. L., Hampton, D. L. & Heavner, M. J. Preliminary results from the sprites 94 aircraft campaign: 2. Blue jets. *Geophys. Res. Lett.* **22,** 1209–1213 (1995).
13. Wescott, E. M., Sentman, D. D., Heavner, M. J., Hampton, D. L. & Vaughan, O. H. Jr Blue jets: Their relationship to lightning and very large hailfall, and their physical mechanisms for their production. *J. Atmos. Solar-Terr. Phys.* **60,** 713–724 (1998).
14. Wescott, E. M. *et al.* New evidence for the brightness and ionization of blue starters and blue jets. *J. Geophys. Res.* **106,** 21549–21554 (2001).
15. Stanley, M. *et al.* High speed video of initial sprite development. *Geophys. Res. Lett.* **26,** 3201–3204 (1999).
16. Gerken, E. A., Inan, U. S & Barrington-Leigh, C. P. Telescopic imaging of sprites. *Geophys. Res. Lett.* **27,** 2637–2640 (2000).
17. Stenbaek-Nielsen, H. C., Moudry, D. R., Wescott, E. M., Sentman, D. D. & Sao Sabbas, F. T. Sprites and possible mesospheric effects. *Geophys. Res. Lett.* **27,** 3827–3831 (2000).
18. Heavner, M. J. *Optical Spectroscopic Observations of Sprites, Blue Jets, and Elves: Inferred Microphysical Processes and their Macrophysical Implications.* Thesis, Univ. Alaska (2000).
19. Moudry, D. R., Stenbaek-Nielsen, H. C., Sentman, D. D. and Wescott, E. M. in *Abstr. National Radio Science Meeting of URSI* G/H3-12, 107 (Boulder, Colorado, 2001).
20. Uman, M. A. *The Lightning Discharge* (Academic, San Diego, 1987).
21. Petrov, N. I. & Petrova, G. N. Physical mechanisms for the development of lightning discharges between a thundercloud and the ionosphere. *Tech. Phys.* **44,** 472–475 (1999).
22. Pasko, V. P., Inan, U. S. & Bell, T. F. Large scale modeling of sprites and blue jets. *Eos* **80,** F218 (1999).
23. Pasko, V. P. & George, J. J. Three-dimensional modeling of blue jets and blue starters. *Eos* **82,** F150 (2001).
24. Hale, L. C., Croskey, C. L. & Mitchell, J. D. Measurements of middle-atmosphere electric fields and associated electrical conductivities. *Geophys. Res. Lett.* **8,** 927–930 (1981).
25. Croskey, C. L., Hale, L. C. & Mitchell, J. D. Electrical stratification in the middle atmosphere. *Adv. Space Res.* **10,** 49–52 (1990).
26. Lyons, W. A., Stanley, M. A., Nelson, T. E. & Taylor, M. Sprites, elves, halos, trolls and blue starters above the STEPS Domain. *Eos* **81,** F131 (2000).
27. Wescott, E. M. *et al.* Starters: Brief upward discharges from an intense Arkansas thunderstorm. *Geophys. Res. Lett.* **23,** 2153–2156 (1996).
28. Sukhorukov, A. I., Mishin, E. V., Stubbe, P. & Rycroft, M. J. On blue jet dynamics. *Geophys. Res. Lett.* **23,** 1625–1628 (1996).
29. Roble, R. G. On modeling component processes in the Earth's global electric circuit. *J. Atmos. Terr. Phys.* **53,** 831–847 (1991).
30. Rycroft, M. J., Israelsson , S. & Price, C. The global atmospheric electric circuit, solar activity and climate change. *J. Atmos. Solar-Terr. Phys.* **62,** 1563–1576 (2000).

Supplementary Information accompanies the paper on *Nature*'s website (http://www.nature.com).

Acknowledgements

The GEN III intensifier was provided by ITT Night Vision Industries; we thank M. Robinson for support of our work. We thank W. Lyons for discussions, and S. Gonzalez, Q. Zhou, M. Sulzer, C. Tepley, J. Friedman, E. Robles, A. Venkataraman and E. Castro for support of our observations at Arecibo Observatory. The Arecibo Observatory is a component of the National Astronomy and Ionosphere Center, which is operated by Cornell University under a cooperative agreement with the National Science Foundation. This work was supported by a Small Grant for Exploratory Research from the National Science Foundation to Pennsylvania State University. Stanford participation was also supported by the Office of Polar Programs of the National Science Foundation.

Competing interests statement

The authors declare that they have no competing financial interests.

Correspondence and requests for materials should be addressed to V.P.P. (e-mail: vpasko@psu.edu) or M.A.S. (e-mail: stanleym@lanl.gov).